HHS Public Access

Author manuscript

Nanomedicine. Author manuscript; available in PMC 2017 February 14.

3D Tumor tissue analogs and their orthotopic implants for understanding tumor-targeting of microenvironment-responsive nanosized chemotherapy and radiation

Pallavi Sethi[1], **Amar Jyoti**[1], **Elden P Swindell**[2], **Ryan Chan**[1], **Ulrich W. Langner**[3], **Jonathan M Feddock**[3], **Radhakrishnan Nagarajan**[4], **Thomas V. O'Halloran**[2], and **Meenakshi Upreti**[1]

[1]Department of Pharmaceutical Sciences, College of Pharmacy, University of Kentucky, Lexington, 789 South Limestone Street, KY, USA

[2]Chemistry of Life Processes Institute, Department of Chemistry, Northwestern University, 2145 Sheridan Road, Evanston, IL 60208-3113.

[3] University of Kentucky Chandler Hospital, Department of Radiation Medicine, 800 Rose Street, Pavilion H Lexington, KY 40536-0293

[4]Division of Biomedical Informatics, University of Kentucky, 725 Rose Street, Multidisciplinary Science Bldg, 230FLexington, KY 40536-0082

Abstract

An appropriate representation of the tumor microenvironment in tumor models can have a pronounced impact on directing combinatorial treatment strategies and cancer nanotherapeutics. The present study develops a novel 3D co-culture spheroid model (3D TNBC) incorporating tumor cells, enodothelial cells and fibroblasts as color-coded murine tumor tissue analogs (TTA) to better represent the tumor milieu of triple negative breast cancer *in vitro*. Implantation of TTA orthotopically in nude mice, resulted in enhanced growth and aggressive metastasis to ectopic sites. Subsequently, the utility of the model is demonstrated for preferential targeting of irradiated tumor endothelial cells via radiation-induced stromal enrichment of Galectin-1 using Anginex conjugated nanoparticles (nanobins) carrying arsenic trioxide and cisplatin. Demonstration of a multimodal nanotherapeutic system and inclusion of the biological response to radiation using an *in vitro/ in vivo* tumor model incorporating characteristics of tumor microenvironment presents an advance in preclinical evaluation of existing and novel cancer nanotherapies.

Graphical Abstract

3D TNBC tumor model of tumor tissue analogs (TTA) *in vitro* and their orthotopic implants to demonstrate radiation guided endothelial cell targeting

Corresponding Author: Meenakshi Upreti 555 Biopharmaceutical Complex College of Pharmacy, University of Kentucky, 789 S. Limestone Street, Lexington, KY 40536-0596, USA m.upreti@uky.edu Phone number: +1-859-218-1041.

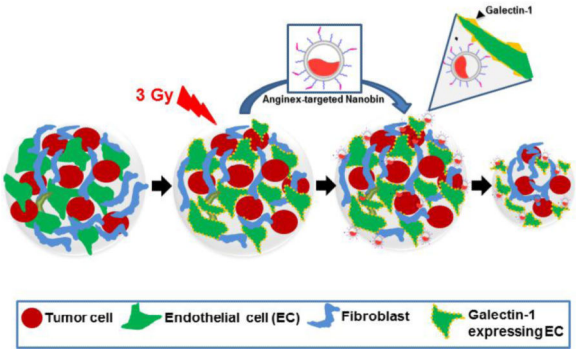

Keywords

Tumor tissue analogs (TTA); Tumor cell spheroids; galectin-1; tumor microenvironment; targeted nanoparticle; 3D co-cultures; 3 dimensional Triple negative breast cancer (3D TNBC) model

Background

Clinical treatment of most cancer types involves some combination of surgery, radiation therapy and chemotherapy. There is a critical need for novel tumor models for investigating multimodal treatment strategies such as those utilizing nanoparticles and radiation. Several studies, including our own, have demonstrated that genetic alterations of tumor cells are not the sole driving force behind tumor development and that tumor growth, metastasis and response to treatment are intimately controlled by the tumor microenvironment [1-3]. Tumor models incorporating aspects of the tumor microenvironment may explain and predict why many therapies do not reach the expected level of activity in the patient.

Penetration of the drugs from nanoparticles across the tumor interstitium and endothelial tissue has been a major challenge in the success of nanoparticles as a treatment modality in cancer. Efforts in evaluating nanoparticles for cancer therapy have also demonstrated a need for more representative *in vitro* and *in vivo* models of human cancer. Nanoparticle therapy is largely dependent on the EPR effect [4] and tissue penetration [5], and therefore it is critical to accurately represent the neovascular architecture of the tumor in preclinical models.

Expanding tumors are the result of an evolving crosstalk between the tumor cell and several nontumoral cells or supportive tumor stroma including the vascular endothelial cells [6] and fibroblasts [7]. This study presents a co-culture system to enable the examination of some of these cell-cell interactions *in vitro*. Utilizing gravity enforced self-aggregation by growing color-coded tumor cells, endothelial cells and fibroblasts in hanging drops of medium *in vitro* we develop tumor tissue analogs (TTA). 3D Cell culture on membrane substrates such as Matrigel [8] and Gelfoam [9] while effective in recreating the tumor biology have not yet been able to replicate the treatment response as observed *in vivo*. The inter-cellular interaction of different cell types in culture medium devoid of growth factors or basement membrane substitutes in the TTA results in a tumor–like microtissue with natural extracellular matrix, enable targeting of the tumor microenvironment and assessment of the impact of a combinatorial nanotherapeutic system. The avascular microtissue or TTA so

developed are implanted orthotopically in the mammary fat pad of mice to model the progression of triple negative breast cancer (TNBC) in an experimentally feasible time span. *In vivo* implantation of the TTA in dorsal skin fold window chambers and the rear limb of mice results in enhanced tumor growth, profuse neovascularization and aggressive metastasis. [2].

An improved understanding of the molecular and structural changes in the tumor microenvironment enhances the ability to study target-based nanotherapeutic interventions. There is compelling evidence that galectin-1 is an important protein in cancer biology with prognostic and predictive value in a spectrum of cancers [10-15]. Galectin-1 is enriched in the tumor-associated stroma or neovascular endothelium [16-19]. Radiation therapy/exposure has been shown to further augment galectin-1 expression in the tumor microenvironment [2,20,21]. The anti-angiogenic 33-amino acid, beta sheet peptide anginex [22,23] specifically binds and inhibits the function of galectin-1 receptor [16-19]. This work utilizes the 3D murine tumor model to study the anginex conjugated liposomal nanoparticles, for selective delivery of cytotoxic payloads of arsenic and cisplatin to the irradiated tumor endothelium via radiation-induced stromal enrichment of Galectin-1. Changes in the fluorescence intensity, spheroid sizing, molecular profiling and immunohistochemistry of color coded TTA are exploited as methods for the therapeutic evaluation of the combinatorial nanotherapeutic strategy *in vitro*. Similar response to the targeting strategy is observed in the TTA implant *in vivo.* In this study the 3D TNBC model, which allows for controlled experimental manipulation in a cost-effective manner, is used to investigate radiation-enhanced targeted nanoparticle uptake in *in vitro* and *in vivo* settings. In summary, this report presents a powerful new tool for studying a breast cancer treatment with clinically critical combinations of radiation and nanochemotherapy and having the potential to accelerate discovery.

Methods

3D Cultures in “Hanging Drop.”

4T1-mcherry tumor cells, C166-GFP endothelial cells and murine embryonic fibroblasts (MEF) were used to generated single or multicell type 3D cultures in “hanging drops” of media (Dulbecco modified Eagle medium with 10% fetal bovine serum and antibiotic mix) as previously described [3] and in supplementary information. The TTA were sized using a phospho imager and TTA of equal size were used in all experimental studies.

Synthesis and characterization of Anginex-Nanobins

Untargeted and alkyne-functional nanobins were synthesized as previously described [24,25] and the synthesis is described in the Supplementary Information. Anginex peptide was syntesised by modifying the peptide at the n-terminus with azide-dPEG$_4$-NHS (Quanta Biodesign). Nanobins were characterized for size and elemental content as described in the supplementary information.

Immunohistochemistry and Microscopy

Equal sized 6-10 TTA and tumor tissues were harvested and frozen in O.C.T (Tissue-Tek, Miles USA, Inc, Elkhart, IN). 5-10 micrometer cryostat sections were

immunohistochemically analyzed using standard protocols. The primary antibody used recognized fibronectin at a dilution of 1:200 and Galectin-1 at a dilution of 1:400. Images were taken at 10X and 40X using a FV1000 laser scanning confocal microscope. Images were processed using FV10-ASW 1.7 viewer software. Images were analyzed using Olympus image analysis software and ImageJ 1.47v (NIH, Bethesda, USA) as 8-bit monochromatic image files. Hematoxylin and eosin staining was performed to assess the tissue-like integrity of 3D cultures. Accumulation of DID labeled nanobins and Sytox blue staining, mCherry- and GFP-expressing cells was imaged using argon lasers at 633nm 406 nm, 532 and 453 nm, respectively.

Light Sheet Microscopy

TTA were imaged18 hr post treatment using a Lightsheet Z.1 microscope (Carl Zeiss Microscopy, Jena, Germany). TTA were embedded in 1% low-melt agarose (Sigma Aldrich, St. Louis, MO) in FluoroBrite™ DMEM (Invitrogen) and placed in CO_2 controlled sample chamber at 37•C. TTA were excited by 488, 561 and 638nm lasers to image the presence of C166-GFP, 4T1-mCherry cells and DID-labelled nanobins respectively. Images were acquired using w-Plan Apochromat 20×/1.0 NA objectives. 280-320 optical sections of 0.233μm thickness with left and right illumination for each sample using ZEISS ZEN imaging software and max intensity fusions were generated. Zero and 180 degree images were fused to reconstruct complete 3D structures.

Animals

All animal procedures were approved by the University of Kentucky Animal Institutional Care and Use Committee (IACUC). Female, athymic, nude mice (CRL) (6-12 weeks old, 20-22gm) were purchased from Harlan's Laboratories (Haslett, MI). All experimental mice were housed in sterile environmental conditions of the University of Kentucky's Division of Laboratory Animal Resources (DLAR) and provided sterile food and water *ad libitum*.

Orthotopic Breast Cancer Model

Mice were anesthetized with isoflurane (1-4% vaporizer) or Ketamine/Xylazine, IP, 100/10 mg/kg respectively. Two 3D tumor cell spheroids or TTA were subcutaneously implanted by a small incision (2-4 mm) bilaterally into the fat pad of the 3rd mammary gland and sutured with tissue adhesive (3M VetBond, St. Paul, MN) Tumor growth was recorded by caliper measurement after a recovery period of 1-2 days. Mice were euthanized at study endpoint by isoflurane overdose. Tumor tissues and lungs were excised for further analysis.

Tumor/Cell X–Ray Irradiation

Radiation exposure was given using the Varian TrueBeam System (Varian medical systems, Palo Alto, CA) X-Ray machine set at a radiation dose rate 1.018±0.10 Gy/min at 150 kV and 6.6 mA. Typical radiation exposure in all experiments was at 3Gy. Mice were anesthetized with Ketamine/Xylazine, IP, 100/10 mg/kg, and radiation was administered with a custom cut lead shielding covering the animal, except for the tumor-bearing region.

Tail Vein Injection

The animals were anesthetized as described above. DID [Dioctadecyltetramethylindodicarbocyanine] labeled nanobins (arsenic concentration 4mg/kg) were administered at a volume of 150-200μl with a 27G needle in the lateral vein of tail.

Phospho MAPK Antibody Array

TTA harvested at day 8 post-treatment and the tumor tissues harvested 24 hr post treatment were homogenized using a 21-gauge syringe in lysis buffer as described earlier [3]. Insoluble material were removed by centrifugation (15 min,12000g). The protein concentration was determined using micro BCA protein assay kit (Thermo scientific Pierce, Rockford, IL). 125 μg of lysate was hybridized to a human phospho MAPK antibody array (R&D Systems Inc, Minneapolis, MN) as instructed.

Pathway Analysis

The Ingenuity Pathway Analysis Tool was used to identify gene networks and examine the functional associations between differentially expressed proteins in the MAPK arrays (www.ingenuity.com).

Inductively coupled plasma-mass spectrometry

Platinum and Arsenic quantification in tumor tissues was accomplished via ICP-MS of acid digested samples using a Thermo XSeries II ICP-MS (Thermo-Fisher Scientific, Waltham, MA) as described [26]. Details provided in Supplementary information.

Statistical Analysis

Data are expressed as mean ± 1 SD of at least three different experiments. Statistical significance of difference in means was performed using parametric two sample t test with unequal variance (α=0.05; GraphPad Prism software). For data analysis of Phospho MAPK antibody arrays, K-means clustering in conjunction with correlation metric was used to partition markers on the array into three clusters based on their expression profile across the three treatment conditions.

Results

Developing tumor tissue analogs from three dimensional (3D) co-cultures *in vitro*

The tumors *in vivo* are not merely an aggregation of cancer cells but are representative of structurally and functionally deregulated organs composed of tumor cells and the microenvironment warranting its incorporation in tumor models. It is important to incorporate this complex structure in models used to study novel cancer therapies. Using a 3D co-culture system designed to replicate aspects of tumor microenvironment that simulate the gradient of micrometastatic growth, we have developed murine breast tumor tissue analogs (TTA) comprised of mCherry fluorescent protein expressing 4T1 tumor cells, GFP expressing C166 endothelial cells and fibroblasts (MEFs). The 3D co-cultures can be maintained for up to 4-6 weeks and continue to grow to the size of an avascular tumor

microtissue (~600 μM). **Fig. 1A** shows confocal and DIC images of the 3D cultures of different cell types that exist in the tumor/tumor microenvironment. More importantly, the co-cultures of tumor cells with endothelial cells **(T+E)** and tumor cells with endothelial cells and fibroblast **(T+E+F)** that were monitored for up to 4 weeks produced a prominent growth in 3D **(Fig. 1A-C)**. In contrast, 3D cultures of any single cell type form an aggregate of cells in a hanging drop that fails to grow beyond 9 days **(Fig. 1A, T & E)**. H & E staining and immunohistochemistry for extracellular matrix proteins like Fibronectin indicate the formation of a tissue-like architecture and natural extracellular matrix in these 3D multicellular co-cultures termed tumor tissue analogs (TTA) **(Fig. 1D)**.

Accelerated growth and aggressive metastasis to the lung in tumors originating form orthotopic implants of TTA

In traditional murine TNBC xenograft models for breast cancer about a million tumor cells are injected orthotopically or in the tail vein of immune-deficient nude mice to develop tumors (400 mm^3) with a neovasculature in 3 weeks and metastasis in 4-6 weeks [27,28] respectively. The experimental design in such tumor models is often unable to meet all the clinical endpoints post-treatment. We have demonstrated the usefulness of the 3D TNBC model in *in vivo* setting by implantation of the TTA in the mammary fat pad of nude mice. Each 3D co-culture is generated from 3000 cells comprising 1-3 different cell types growing in a 'hanging drop' of medium. While the 3D tumor cell aggregates **(T)** generated from 3000 mCherry 4T1 tumor cells develop slow-growing tumors ~200 mm^3 in size with no metastasis to the lung when implanted orthotopically in nude mice, tumors originating from tumor-endothelial cell **(T+E)** or tumor-endothelial-fibroblast **(T+E+F)** TTA grow to ~1500 mm^3 in size and exhibit aggressive metastasis to the lung by 20-24 days **[Fig. 2]**.

The tumor cell population when the 3D cultures are initiated is 100% in tumor cell aggregates **[T]**, 50% in **T+E** and 33% in **T+E+F** TTA with a total of 3000 cells in each hanging drop of medium. Interestingly, the tumor cell population was also found to be higher in tumor-bearing mice with tumors originating from the 3D tumor cell aggregates compared to tumors originating from TTA generated from 3D co-cultures. The tumor tissues originating from tumor cell spheroids **[T]** have a tumor cell population (~17%) while tumor tissue from TTAs **[T+E]** (~13%) and **[T+E+F]** (~10%) **[Fig. 2C]** Although the tumor cell population is higher in the *in vitro* 3D cultures and in tumors originating from tumor cell aggregates **(T),** the tumor growth and metastasis to the lungs was observed to be markedly pronounced in the mice bearing implants of TTA **(T+E/T+E+F) [Fig 2A]**. We expect the tumor microenvironment to enhance the invasive or stem-cell phenotype of the tumor cells [29,30] thereby causing them to metastasize to the lung. These results elucidate upon the predominant role of the stromal components in the tumor progression and invasion in this disease model.

Radiation exposure augments expression of galectin-1 in endothelial cells of the tumor microenvironment

The development of receptor-targeted nanoparticle delivery has been particularly challenging and one of the major obstacles is in identifying cell surface biomarkers that are expressed sufficiently in the tumor and/or tumor microenvironment. Our earlier study has

reported a surge in the expression of Galectin-1 upon radiation exposure as low as 0.5 Gy in membranous fractions of human and murine endothelial cell types [2]. We have generated new evidence that this increase in galectin-1 expression upon radiation exposure occurs in endothelial cells comprised in the tumor microenvironment. The murine endothelial cell lines (2H11 and C166), when incubated in conditioned medium from 4T1 murine breast cancer cells that is expected to mimic the tumor microenvironment, express higher levels of galectin-1 with changes in morphology. The galectin-1 expression is further augmented in endothelial cells, including the cell surface upon radiation exposure. The phenomenon of galectin-1 expression and surge upon radiation exposure is not observed in endothelial cells grown in serum free medium *in vitro* and is expected to simulate the quiescent phenotype of endothelial cells that exist in the vasculature of normal tissues *in vivo* **[Fig. 3]**. Fibroblasts are another cell type present in the tumor microenvironment. Galectin-1 expression in murine embryonic fibroblast (MEFs) incubated in normal, serum free or conditioned medium was also analyzed by immunohistochemistry. In all culture conditions galectin-1 in the MEFs with or without radiation exposure **[S1]** was not noticeable.

Nanotherapeutic strategy to target the radiation stimulated tumor endothelium

The clinical applications of FDA-approved arsenic (Trisenox) and cisplatin (Platinol) based therapies are limited by inadequate drug delivery to tumors resulting in dose-limiting systemic toxicities, rapid drug clearance, and acquired drug resistance by tumor cells. Nanoparticle encapsulation improves the circulation half-life of arsenic trioxide [26,31]. Furthermore, addition of a targeting ligand (uPAR) improves the anti-tumor effect of arsenic loaded nanoparticles [25]. Galectin-1 is a specific receptor for the antiangiogenic peptide anginex [19], and its radiation-responsive expression makes it a promising candidate for actively targeting irradiated tumors with anginex-conjugated nanoparticles [2]. Liposomes loaded with arsenic trioxide [31-33], are conjugated to anginex for targeting the irradiated TTA and tumors originating from their orthotopic implants *in vivo*. These nanocarriers utilize cisplatin ions to form nanoparticulate complexes with arsenic trioxide inside a 80 nm lipid membrane. The conjugation of anginex to the nanoparticles, occurs in three steps **(Fig. 4)**. First, the anginex is modified with a heterobifunctional crosslinker containing an azide group. Next, drug-loaded nanoparticles are modified with an alkyne-containing lipid molecule, creating alkyne-modified reactive nanoparticles. The alkyne nanobins and the azide anginex are then cross-linked using a copper-catalyzed alkyne-azide cycloaddition or "click" reaction [34]. The resulting nanoparticles are characterized by ICP-OES to determine arsenic, platinum and phospholipid content. The anginex-nanobins were measured to be 80.3 nm, slightly larger and more polydisperse than the non-conjugated/untargeted nanoparticles **(Supplementary material Table. 1).**

The 3D TNBC model allows targeting of the tumor endothelium and assessment of the impact of the combinatorial nanotherapeutic system

A radiation stimulated tumor microenvironment was developed using the TTA to study the targeted delivery of nanoparticles over an extended period of time (8 days). The combination of targeted nanobins and radiation caused pronounced elimination of the GFP labeled endothelial cells **(green)** in the TTA **[T+E+F](Fig. 5A)**. The untargeted nanobins

did not result in similar effect on endothelial cells (green) in the non-irradiated or irradiated TTA.

The enhanced cytotoxic effect of anginex-conjugated nanobins at 5 μM concentration was validated by evaluating the extent of cell permeation by sytox blue staining in irradiated TTA at 8 days post treatment **(Fig. 5B, E & F)**. Sytox blue is a fluorescent nuclear and chromosome counterstain with an emission maxima at 480 nm that is impermeant to live cells, making it a useful indicator of dead cells within a population. Similar results of decrease in endothelial cell fluorescence and enhanced cell damage with sytox blue staining upon the same treatment conditions with the anginex-conjugated nanobin post-radiation exposure (day 8) were observed in TTA developed from 3D co-cultures of tumor cells and endothelial cells **[T+E] (Fig 5C & D)**. Accumulation of far-red fluorescing DID-labeled anginex conjugated nanobins (**Purple**) on irradiated TTA when imaged at an excitation wavelength of 638 nm assessed by light sheet microscopy (LSM) was also higher than the non-targeted nanobins **(Fig. 5G)**.

In vivo irradiation of tumors from orthotopic implants of TTA increases galectin-1 expression and nanobin uptake

We have demonstrated the induction of galectin-1 expression in tumor-associated endothelial cells upon radiation exposure in 2D monolayer cell cultures and 3D co-cultures *in vitro* [**Fig. 1** and [3]]. A similar pattern of increase in galectin-1 in response to radiation exposure is also observed in the murine TNBC model developed from orthotopic implants of TTA [**Fig. 6A**]. The pattern of nanoparticle accumulation and drug uptake upon treatment with anginex-conjugated nanobins following radiation therapy was also noticeably higher in irradiated tumor tissue analogs **(T+E+F)** grown orthotopically in nude mice compared to other combinations of tumor implant and drug targeting **(Fig. 6)**.

Accumulation of arsenic and cisplatin analyzed by inductively coupled plasma mass spectrometry (ICP-MS) was also found to be significantly higher in tumor tissue samples originating from TTA (**T+E+F)** grown *in vivo* **(Fig. 6B-C). Fig. 6D-E** elucidates the radiation enhanced targeting of anginex-conjugated nanobins and drug uptake in tumors from TTA (**T+E+F)** grown *in vivo*.

Enhanced cytotoxicity to the combinatorial nanotherapeutic strategy occurs by alteration in apoptotic and stress signaling via the activation/phosphorylation (S46) of functional p53 in the targeted endothelial cells

Alterations in intercellular kinases in response to the nanotherapeutic strategy was assessed by probing Phopho MAPK arrays (R & D systems) **[Fig. 7A]**. Elevated phosphorylation of 26 proteins was observed in the irradiated TTA **(T+E+F)** that were incubated with galectin-1 targeted nanobins compared to irradiated TTA incubated with unconjugated nanobins or vehicle alone. Proteins exhibiting changes in phosphorylation were grouped into three clusters revealed by k-means clustering **(Fig. 7B-C)**. Proteins in cluster 1 (ERK2, GSK3aß, MKK3, MKK6, RSK1, RSK2, TOR) are activated by both targeted and untargeted treatment. Members of cluster 2 (Akt1, Akt2, HSP27, JNK1, p38a, p53) are activated only by targeted nanoparticle treatment. Members of cluster 3 (Akt3, Aktpan, CREB, ERK1,

GSK3ß, JNK2, JNK3, JNKpan, MSK2, p38ß, p38d, p38, p70S6Kinase) are strongly activated by targeted nanoparticle treatment and only partially activated by untargeted nanoparticle treatment (**Fig. 7B)**. Of particular interest is the activation of cluster 2 protein p53, which regulates apoptosis as a result of DNA damage and cellular stress. A similar semi-quantitavtive comparison was performed for assessing the changes in protein phosphorylation in the tumor tissue analogs **(T+E+F)** that were incubated with anginex-conjugated nanobins with and without radiation exposure (3Gy) **(S2A)**. A heat-map generated from the array quantification revealed elevated expression of phosphorylated proteins like AKT1, AKT3, JNK1, JNK2, JNK3 MKK3, p38γ and p53 **(S2B)** in response to radiation and stress [35-37].

TTA grown *in vivo* were also analyzed using the semi-quantitative phospho-MAPK protein array. Heatmaps generated from quantification of pixel densities of phosphoproteins demonstrated a greater that 5-fold activation of proteins such as AKT1, AKT3, JNK1, JNK2, JNK3 MKK3, p38γ and p53 in response to radiation combined with nanotherapy **(Fig. 7D)**. The Ingenuity pathway analysis (IPA) revealed the enhanced activation/ phosphorylation of these proteins to be associated with apoptosis/stress signaling occurring via the phosphorylation of p53 (S46), which is important for the amplification of apoptotic signals **(Fig. 7E)**. We therefore expect that higher uptake of anginex-conjugated nanobins via endothelial galectin-1 triggers phosphorylation of p53 and the apoptotic and stress signaling cascade in the murine tumor model. This results in subsequent killing of the tumor cells and other cells types in the neighboring microenvironment. The 4T1 murine breast carcinoma cells are p53 null/deficient [38] and do not contribute directly to cell killing mediated by phosphorylation of functional p53. These findings indicate the importance of tumor microenvironment in directing drug delivery and treatment response in tumors. This is the first study attempting to understand a novel combinatorial nanotherapeutic system in an *in vitro/ in vivo* tumor model that incorporates stromal features and establishes a convincing connection between the *in vitro* and *in vivo* findings.

Discussion

The need for more robust models incorporating the tumor microenvironment has affected the efforts in evaluating nanoparticles for cancer therapy. Nanoparticle therapy is largely dependent on the EPR effect [4], and so it is critical to accurately represent the neovascular architecture of the tumor in preclinical models. Attempts in this direction, conducted in 2D monolayer cell cultures do not reflect response to nanoparticle toxicities at tissue levels in animals [39]. Here we demonstrate a new preclinical 3D TNBC model system that allows us to comprehensively evaluate a novel combinatorial system for nanotherapeutics against an environment similar to occult cancer. The color-coded 3D TNBC model utilizing the TTA developed in this study incorporates critical aspects of the tumor microenvironment that impact tumor progression and invasion, and also lends itself to high-throughput controlled manipulation in a way that other tumor models do not. Our results clearly elucidate that the sensitivity to low concentrations (5 μM) of endothelial cell-targeted (ax-conjugated) nanobins following radiation exposure can be monitored and validated with TTA *in vitro* using confocal microscopy along with staining for sytox blue, a fluorescent dye to detect cell damage, before moving to more expensive animal models. These findings have led us to

establish that the increased sensitivity of TTA to ax-conjugated nanobins is as a consequence of radiation-guided preferential targeting of green fluorescent protein (GFP) expressing endothelial cells **(Fig. 5)**.

The semiquantitative phospho MAPK antibody array, was used to elucidate the impact of the radiation-guided nanotherapeutic targeting strategy in triggering a stress and cell death signaling response via the activation and phosphorylation of p53 at the serine 46 (Ser^{46}) residue in TTA and their orthotopic implants *in vivo* **(Fig. 7)**. It is important to note that among the post translational modifications specifically linked to apoptosis in normal cells is phosphorylation of p53 at $Ser^{4640-43}$. Apoptotic stress induced by cisplatin has also been shown to affect the phosphorylation/modulation of p53 via activation of p38, JNK and MKK3 [44-48]. Cellular stress, including DNA damage by ionizing radiation has been shown to accelerate senescence in endothelial cells via AKT activation and subsequent phosphorylation of p53 [49-51]. Most tumor-derived cell lines are either p53 deficient, defective or aberrant in p53 signaling such as 4T1 murine breast adenocarcinoma cells that are p53 null/deficient [38]. Since functional p53 is expressed only in the endothelial cells and fibroblasts, we expect the pronounced cell damage observed in the TTA to be a consequence of the radiation-guided targeting of anginex-conjugated nanobins in endothelial cells. These molecular findings utilizing a tumor model system that better recapitulate the human tumor microenvironment demonstrate the utility of targeting the tumor endothelium as a potential for combinatorial cancer therapy.

While 3D multicellular tumor cell spheroids have been in use as *in vitro* tumor models for optimization of intratumoral nanoparticle or drug delivery [52-54] extending the *in vitro* findings to *in vivo* settings has proven to be elusive. The present study is significant because it demonstrates a mechanistic handshake between *in vitro* and *in vivo* findings and enable evaluation of existing and novel combinatorial cancer nanotherapies.

Supplementary Material

Refer to Web version on PubMed Central for supplementary material.

Acknowledgments

Supported by: National Cancer Institute grants R21CA173609 to M.U, R25CA153954 and Cancer Nanotechnology Platform Partnership U01CA151461 to T.V.O.

Metal analysis was performed at the NU Quantitative Bio-elemental Imaging Center (QBIC) generously supported by NASA Ames Research Center NNA06CB93G.

References

1. Neri D, Bicknell R. Tumour vascular targeting. Nature reviews. Cancer. 2005; 5:436–446. doi: 10.1038/nrc1627. [PubMed: 15928674]
2. Upreti M, et al. Radiation-induced galectin-1 by endothelial cells: a promising molecular target for preferential drug delivery to the tumor vasculature. Journal of molecular medicine. 2013; 91:497–506. doi:10.1007/s00109-012-0965-1. [PubMed: 23090010]
3. Upreti M, et al. Tumor-Endothelial Cell Three-dimensional Spheroids: New Aspects to Enhance Radiation and Drug Therapeutics. Translational oncology. 2011; 4:365–376. [PubMed: 22191001]

4. Maeda H, Nakamura H, Fang J. The EPR effect for macromolecular drug delivery to solid tumors: Improvement of tumor uptake, lowering of systemic toxicity, and distinct tumor imaging in vivo. Adv Drug Deliv Rev. 2013; 65:71–79. doi:10.1016/j.addr.2012.10.002. [PubMed: 23088862]
5. Barua S, Mitragotri S. Challenges associated with Penetration of Nanoparticles across Cell and Tissue Barriers: A Review of Current Status and Future Prospects. Nano today. 2014; 9:223–243. doi:10.1016/j.nantod.2014.04.008. [PubMed: 25132862]
6. Franses JW, Baker AB, Chitalia VC, Edelman ER. Stromal endothelial cells directly influence cancer progression. Science translational medicine. 2011; 3:66ra65. doi:10.1126/scitranslmed.3001542.
7. Kalluri R, Zeisberg M. Fibroblasts in cancer. Nature reviews. Cancer. 2006; 6:392–401. doi:10.1038/nrc1877. [PubMed: 16572188]
8. Lee GY, Kenny PA, Lee EH, Bissell MJ. Three-dimensional culture models of normal and malignant breast epithelial cells. Nature methods. 2007; 4:359–365. doi:10.1038/nmeth1015. [PubMed: 17396127]
9. Tome Y, et al. 3-dimensional tissue is formed from cancer cells in vitro on Gelfoam(R), but not on Matrigel. Journal of cellular biochemistry. 2014; 115:1362–1367. doi:10.1002/jcb.24780. [PubMed: 24497277]
10. Mundt F, et al. Proteome screening of pleural effusions identifies galectin 1 as a diagnostic biomarker and highlights several prognostic biomarkers for malignant mesothelioma. Molecular & cellular proteomics : MCP. 2014; 13:701–715. doi:10.1074/mcp.M113.030775. [PubMed: 24361865]
11. von Klot CA, et al. Galectin-1 and Galectin-3 mRNA expression in renal cell carcinoma. BMC clinical pathology. 2014; 14:15. doi:10.1186/1472-6890-14-15. [PubMed: 24708743]
12. Carlini MJ, et al. Clinical relevance of galectin-1 expression in non-small cell lung cancer patients. Lung cancer. 2014; 84:73–78. doi:10.1016/j.lungcan.2014.01.016. [PubMed: 24560493]
13. Wu TF, et al. Galectin-1 Dysregulation Independently Predicts Disease-Specific Survival In Urinary Bladder Urothelial Carcinoma. The Journal of urology. 2014 doi:10.1016/j.juro.2014.09.107.
14. Camby I, Le Mercier M, Lefranc F, Kiss R. Galectin-1: a small protein with major functions. Glycobiology. 2006; 16:137R–157R.
15. Dalotto-Moreno T, et al. Targeting galectin-1 overcomes breast cancer-associated immunosuppression and prevents metastatic disease. Cancer research. 2013; 73:1107–1117. doi:10.1158/0008-5472.CAN-12-2418. [PubMed: 23204230]
16. Thijssen VL, et al. Tumor cells secrete galectin-1 to enhance endothelial cell activity. Cancer research. 2011; 70:6216–6224. [PubMed: 20647324]
17. Thijssen VL, Hulsmans S, Griffioen AW. The galectin profile of the endothelium: altered expression and localization in activated and tumor endothelial cells. The American journal of pathology. 2008; 172:545–553. [PubMed: 18202194]
18. Thijssen VL, Poirier F, Baum LG, Griffioen AW. Galectins in the tumor endothelium: opportunities for combined cancer therapy. Blood. 2007; 110:2819–2827. [PubMed: 17591944]
19. Thijssen VL, et al. Galectin-1 is essential in tumor angiogenesis and is a target for antiangiogenesis therapy. Proceedings of the National Academy of Sciences of the United States of America. 2006; 103:15975–15980. [PubMed: 17043243]
20. Kuo P, et al. Galectin-1 mediates radiation-related lymphopenia and attenuates NSCLC radiation response. Clin Cancer Res. 2014; 20:5558–5569. doi:10.1158/1078-0432.CCR-14-1138. [PubMed: 25189484]
21. Le QT, Shirato H, Giaccia AJ, Koong AC. Emerging Treatment Paradigms in Radiation Oncology. Clin Cancer Res. 2015 doi:10.1158/1078-0432.CCR-14-1191.
22. Griffioen AW, et al. Anginex, a designed peptide that inhibits angiogenesis. The Biochemical journal. 2001; 354:233–242. [PubMed: 11171099]
23. Mayo KH, van der Schaft DW, Griffioen AW. Designed beta-sheet peptides that inhibit proliferation and induce apoptosis in endothelial cells. Angiogenesis. 2001; 4:45–51. [PubMed: 11824378]

24. Chen H, et al. Coencapsulation of arsenic- and platinum-based drugs for targeted cancer treatment. Angew Chem Int Ed Engl. 2009; 48:9295–9299. doi:10.1002/anie.200903655. [PubMed: 19894238]
25. Zhang Y, et al. Urokinase plasminogen activator system-targeted delivery of nanobins as a novel ovarian cancer therapy. Mol Cancer Ther. 2013; 12:2628–2639. doi: 10.1158/1535-7163.MCT-13-0204. [PubMed: 24061648]
26. Ahn RW, et al. A novel nanoparticulate formulation of arsenic trioxide with enhanced therapeutic efficacy in a murine model of breast cancer. Clin Cancer Res. 2010; 16:3607–3617. doi: 10.1158/1078-0432.CCR-10-0068. [PubMed: 20519360]
27. Gil M, Seshadri M, Komorowski MP, Abrams SI, Kozbor D. Targeting CXCL12/CXCR4 signaling with oncolytic virotherapy disrupts tumor vasculature and inhibits breast cancer metastases. Proceedings of the National Academy of Sciences of the United States of America. 2013; 110:E1291–1300. doi:10.1073/pnas.1220580110. [PubMed: 23509246]
28. Miao Z, et al. CXCR7 (RDC1) promotes breast and lung tumor growth in vivo and is expressed on tumor-associated vasculature. Proceedings of the National Academy of Sciences of the United States of America. 2007; 104:15735–15740. doi:10.1073/pnas.0610444104. [PubMed: 17898181]
29. Borovski T, De Sousa EMF, Vermeulen L, Medema JP. Cancer stem cell niche: the place to be. Cancer Res. 2011; 71:634–639. doi:10.1158/0008-5472.CAN-10-3220. [PubMed: 21266356]
30. Ye J, Wu D, Wu P, Chen Z, Huang J. The cancer stem cell niche: cross talk between cancer stem cells and their microenvironment. Tumour Biol. 2014; 35:3945–3951. doi:10.1007/s13277-013-1561-x. [PubMed: 24420150]
31. Ahn RW, et al. Nano-encapsulation of arsenic trioxide enhances efficacy against murine lymphoma model while minimizing its impact on ovarian reserve in vitro and in vivo. PLoS One. 2013; 8:e58491. doi:10.1371/journal.pone.0058491. [PubMed: 23526987]
32. Chen H, et al. Lipid encapsulation of arsenic trioxide attenuates cytotoxicity and allows for controlled anticancer drug release. J Am Chem Soc. 2006; 128:13348–13349. doi:10.1021/ja064864h. [PubMed: 17031934]
33. Chen H, Ahn R, Van den Bossche J, Thompson DH, O'Halloran TV. Folate-mediated intracellular drug delivery increases the anticancer efficacy of nanoparticulate formulation of arsenic trioxide. Molecular cancer therapeutics. 2009; 8:1955–1963. doi:10.1158/1535-7163.MCT-09-0045. [PubMed: 19567824]
34. Kolb HC, Finn MG, Sharpless KB. Click Chemistry: Diverse Chemical Function from a Few Good Reactions. Angew Chem Int Ed Engl. 2001; 40:2004–2021. [PubMed: 11433435]
35. Davis RJ. Signal transduction by the JNK group of MAP kinases. Cell. 2000; 103:239–252. [PubMed: 11057897]
36. Kang YH, Lee SJ. Role of p38 MAPK and JNK in enhanced cervical cancer cell killing by the combination of arsenic trioxide and ionizing radiation. Oncol Rep. 2008; 20:637–643. [PubMed: 18695917]
37. Verheij M, et al. The role of the stress-activated protein kinase (SAPK/JNK) signaling pathway in radiation-induced apoptosis. Radiother Oncol. 1998; 47:225–232. [PubMed: 9681884]
38. Sang H, et al. Murine mammary adenocarcinoma cells transfected with p53 and/or Flt3L induce antitumor immune responses. Cancer Gene Ther. 2005; 12:427–437. doi:10.1038/sj.cgt.7700809. [PubMed: 15678151]
39. Luo Y, et al. Three-dimensional microtissue assay for high-throughput cytotoxicity of nanoparticles. Anal Chem. 2012; 84:6731–6738. doi:10.1021/ac301191j. [PubMed: 22747067]
40. Oda K, et al. p53AIP1, a potential mediator of p53-dependent apoptosis, and its regulation by Ser-46-phosphorylated p53. Cell. 2000; 102:849–862. [PubMed: 11030628]
41. Rinaldo C, et al. MDM2-regulated degradation of HIPK2 prevents p53Ser46 phosphorylation and DNA damage-induced apoptosis. Mol Cell. 2007; 25:739–750. doi:10.1016/j.molcel.2007.02.008. [PubMed: 17349959]
42. Taira N, Nihira K, Yamaguchi T, Miki Y, Yoshida K. DYRK2 is targeted to the nucleus and controls p53 via Ser46 phosphorylation in the apoptotic response to DNA damage. Mol Cell. 2007; 25:725–738. doi:10.1016/j.molcel.2007.02.007. [PubMed: 17349958]

43. Smeenk L, et al. Role of p53 serine 46 in p53 target gene regulation. PLoS One. 2011; 6:e17574. doi:10.1371/journal.pone.0017574. [PubMed: 21394211]
44. Bragado P, Armesilla A, Silva A, Porras A. Apoptosis by cisplatin requires p53 mediated p38alpha MAPK activation through ROS generation. Apoptosis. 2007; 12:1733–1742. doi:10.1007/s10495-007-0082-8. [PubMed: 17505786]
45. Hernandez Losa J, et al. Role of the p38 MAPK pathway in cisplatin-based therapy. Oncogene. 2003; 22:3998–4006. doi:10.1038/sj.onc.1206608. [PubMed: 12821934]
46. Mansouri A, et al. Sustained activation of JNK/p38 MAPK pathways in response to cisplatin leads to Fas ligand induction and cell death in ovarian carcinoma cells. J Biol Chem. 2003; 278:19245–19256. doi:10.1074/jbc.M208134200. [PubMed: 12637505]
47. Shi Y, et al. ROS-dependent activation of JNK converts p53 into an efficient inhibitor of oncogenes leading to robust apoptosis. Cell Death Differ. 2014; 21:612–623. doi:10.1038/cdd.2013.186. [PubMed: 24413150]
48. Watanabe J, et al. Dicoumarol potentiates cisplatin-induced apoptosis mediated by c-Jun N-terminal kinase in p53 wild-type urogenital cancer cell lines. Oncogene. 2006; 25:2500–2508. doi:10.1038/sj.onc.1209162. [PubMed: 16518417]
49. Miyauchi H, et al. Akt negatively regulates the in vitro lifespan of human endothelial cells via a p53/p21-dependent pathway. EMBO J. 2004; 23:212–220. doi:10.1038/sj.emboj.7600045. [PubMed: 14713953]
50. Panganiban RA, Day RM. Inhibition of IGF-1R prevents ionizing radiation-induced primary endothelial cell senescence. PLoS One. 2013; 8:e78589. doi:10.1371/journal.pone.0078589. [PubMed: 24205274]
51. Gottlieb TM, Leal JF, Seger R, Taya Y, Oren M. Cross-talk between Akt, p53 and Mdm2: possible implications for the regulation of apoptosis. Oncogene. 2002; 21:1299–1303. doi:10.1038/sj.onc.1205181. [PubMed: 11850850]
52. Kim B, et al. Tuning payload delivery in tumour cylindroids using gold nanoparticles. Nat Nanotechnol. 2010; 5:465–472. doi:10.1038/nnano.2010.58. [PubMed: 20383126]
53. Minchinton AI, Tannock IF. Drug penetration in solid tumours. Nature reviews. Cancer. 2006; 6:583–592. doi:10.1038/nrc1893. [PubMed: 16862189]
54. Wang X, et al. Doxorubicin delivery to 3D multicellular spheroids and tumors based on boronic acid-rich chitosan nanoparticles. Biomaterials. 2013; 34:4667–4679. doi:10.1016/j.biomaterials.2013.03.008. [PubMed: 23537667]

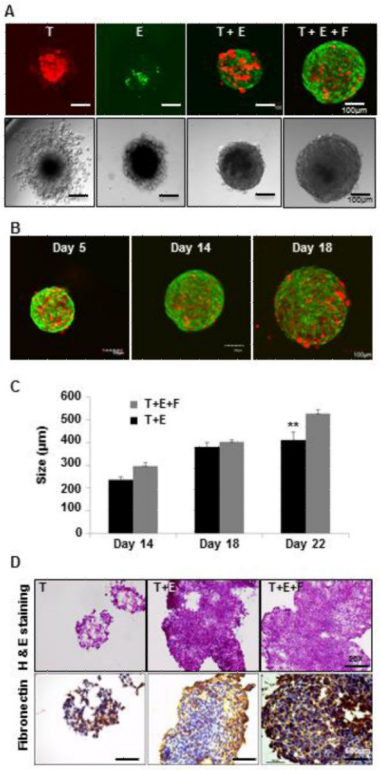

Figure 1. Murine TTA from multicell 3D co-cultures *in vitro* demonstrate robust growth and tissue-like morphology

Confocal **(Upper panel)** and DIC **(Lower panel)** images of 3D cultures at day 14 in hanging drops of medium of **(A)** mCherry (Red) 4T1 tumor cells only **[T],** GFP-C166 endothelial cell only **[E]**, co-culture of tumor cells and endothelial cells **[T+E]**, and co-culture of murine Tumor cells, endothelial cells and mouse embryonic fibroblasts (MEF) **[T+E+F]. (B)** TTA **[T+E+F]** at day 5, 14 and 18. Confocal images are an overlay of green (C166 endothelial cells) and Red (4T1 tumor cells) fluorescence. **(C)** Growth comparison of **[T+E]** and **[T+E+F]** TTA; **(D)** H&E **(Upper panel)** and immunostaining for extracellular matrix protein (fibronectin) **(Lower panel)** in tumor cell aggregates **[T]** and TTA **[T+E, T+E+F]** at 20X magnification.

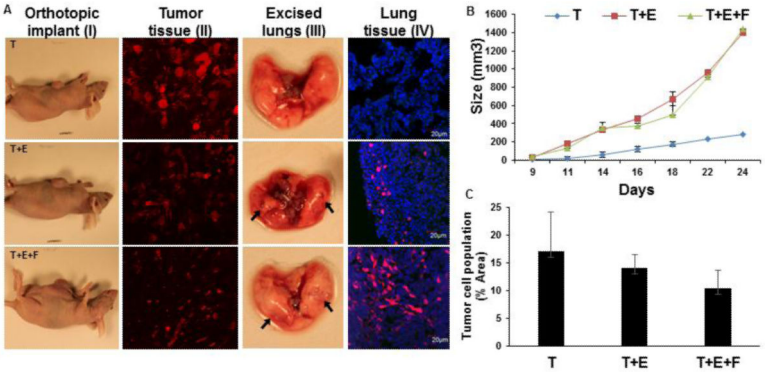

Figure 2. Enhanced growth and metastasis of tumors originating from orthotopic xenografts of 3D TTA

(A) Athymic nude mice bearing mammary fat pad orthotopic tumors originating from 3D cultures (TTA) of 4T1 tumor cells **[T]**, 4T1 tumor and C166 endothelial cells **[T+E]** and 4T1 tumor, C166 endothelial and MEF **[T+E+F] (I);** 4T1 mCherry expressing tumor cells in tissue sections from tumors originating from orthotopic tumors as described earlier **(II)**; Metastasis in diseased lung excised 24 days post-implantation **(III)**, and presence of mCherry 4T1 tumor cells **(Red)** cryosections of lung tissue **(IV)** was found to be more aggressive in tumors originating from **[T+E]** or **[T+E+F]** TTA. **(B)** Tumor growth curve in orthotopic xenografts (n=8) of 3D cultures. Error bars represent mean ± SEM. **(C)** Reduced tumor cell population in Tumor tissue sections of orthotopic xenografts of 3D TTA. The mCherry (red) fluorescent protein expressing tumor cell population in tumor tissues originating from orthotopic xenografts of **[T], [T+E] and [T+E+F]** was quantified by densitomentry using the ImageJ software and graphically represented. Error bars represent mean ± SEM.

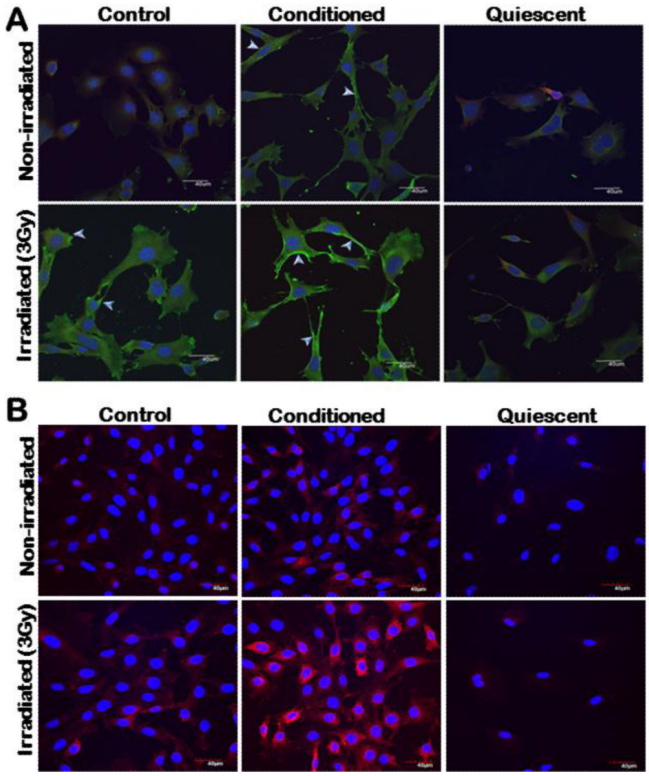

Figure 3. Radiation exposure augments expression of galectin-1 including the cell surface in murine endothelial cells when incubated in conditioned medium from tumor cells

(A) 2H11 and **(B)** C166 endothelial cells grown in regular (control), serum free (quiescent) and conditioned medium from 4T1 murine breast carcinoma cells respectively (upper panel) were subjected to 3Gy of radiation exposure (lower panel). Cells were incubated with goat anti-galectin-1 primary antibody (Invitrogen) followed by incubation with secondary alexafluor 488 (Invitrogen) **[Green]** in 2H11 cells and secondary alexafluor 633 **[Red]** in C166 cells. Nuclei were stained with DAPI **[Blue]**. Scale bar, 40 μm. While there is profuse overexpression of galectin-1 in both endothelial cell types maintained in conditioned medium, the white arrows in 2H11 cells indicate higher accumulation of galectin-1 on endothelial cell surface. Galectin-1 expression in cells grown in serum free condition representative of quiescent/normal endothelial cell phenotype with and without radiation exposure was not noticeable.

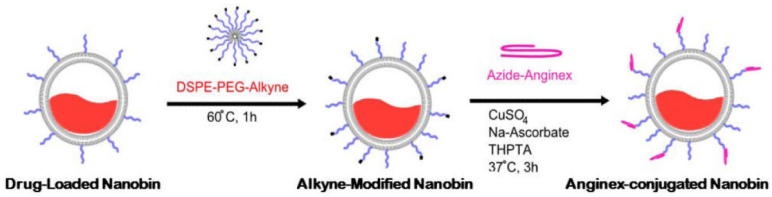

Figure 4. Anginex labeling strategy and for arsenic-cisplatin dual drug loaded nanoparticles

The figure is a schematic of the anginex labeling strategy.

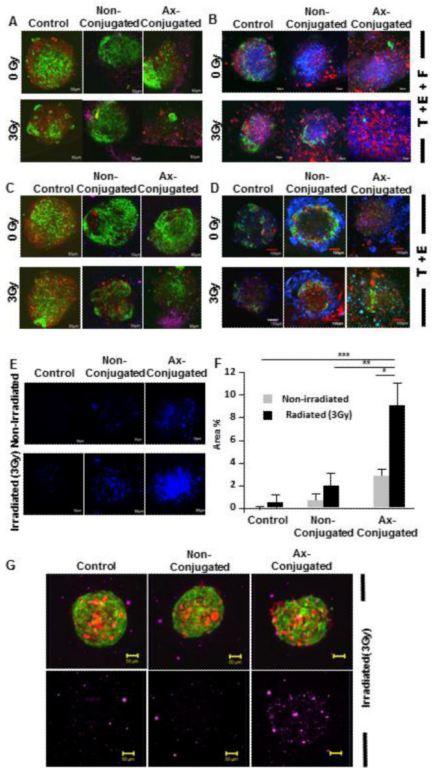

Figure 5. Elimination of endothelial cells (green), increased cell damage and enhanced nanoparticle uptake in tumor tissue analogs (T+E+F) resulting from radiation induced targeting of anginex conjugated arsenic-cisplatin (as-cs) loaded nanobins

Confocal images (10X) of TTAs of **[T+E+F] (A)** and **[T+E] (C)** respectively 48 hr post-incubation with Axconjugated and non-conjugated as-cs loaded nanobins (15 μM) following radiation exposure (3Gy). The nanobins were labeled with a far red fluorescent lipophilic carbocyanine dye, DID. The images are an overlay of **Red** (tumor cells), **Green** (Endothelial cells) and **Purple** (DID labelled nanobins) fluorescence. An overlay of confocal images (10X) of tumor tissue analogs of **[T+E+F] (B)** and **[T+E] (D)** 8 days post-incubation with Ax-conjugated and non-conjugated ascs loaded nanobins **(5 μM)** with and without radiation exposure (3Gy) stained with Sytox blue (nuclear stain for cell damage). The images are an overlay of red (tumor cells), green (endothelial cells) and blue (Sytox blue) fluorescence. **(E)** Representative images of cell damage upon treatment as indicated by Sytox blue staining. **(F)** Toxicity of the radiation induced targeting of nanobins was evaluated by quantitation of the sytox blue staining using an ImageJ software. ***, $P < 0.0001$; **, $P = 0.0006$; *, $P = 0.0004$. **(G)** A comparison of an overlay of images from light sheet microscopy (LSM) excited with purple (DID labeled nanobins) fluorescence of irradiated TTA at 18 hr post treatment.

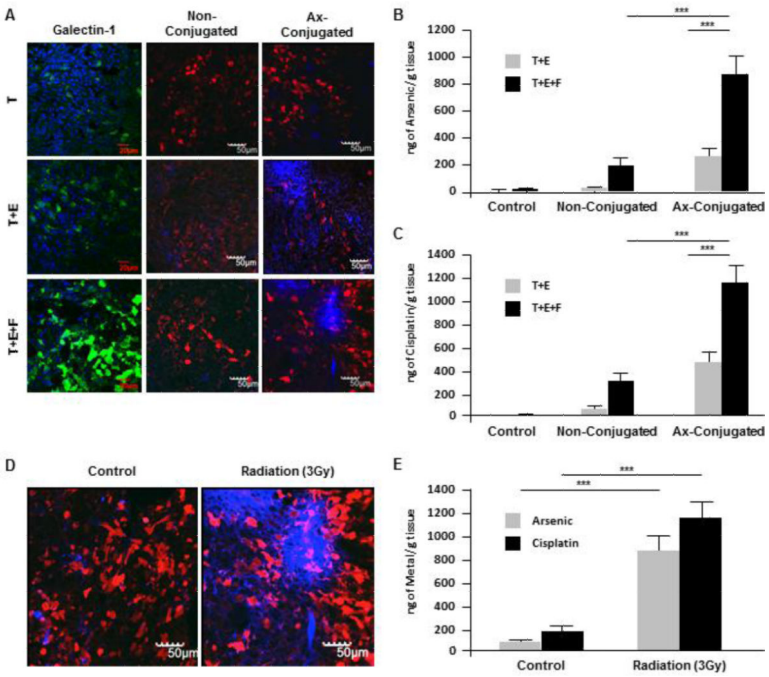

Figure 6. Elevated galectin-1 and Nanobin accumulation with significant drug uptake in orthotopic tumors originating from TTA (T+E+F)

Mice bearing orthotopic tumors originating from 3D tumor cell aggregates **(T)** and tumor tissue analogs of tumor-endothelial cells **(T+E)** and tumor-endothelial cells-Fibroblasts **(T +E+F)** were were exposed to radiation (3Gy) for 4 hr and then injected via tail vein with 4mg/kg of ax-conjugated or non-conjugated arsenic-cisplatin loaded nanobins (DID labelled). **(A)** Confocal images (10X) of tumor tissue sections after radiation exposure and immunostaining with galectin-1 **(left panel)**; followed by incubation with non-conjugated **(middle panel)** and ax-conjugated **(right panel)** nanobins. The images are an overlay of **red** fluorescence (4T1-mCherry tumor cells) and nanobins labelled with DID fluorescing **blue**. ICP-MS analysis of arsenic **(B)** and cisplatin **(C)** concentration in tumor tissues of mice bearing **T+E** and **T+E+F** implants when treated with radiation and ax-conjugated or non-conjugated nanoparticles ***, $P < 0.001$. **(D)** Representative confocal images of tumor tissue sections and their ICP-MS analysis **(E)** for arsenic and cisplatin from **T+E+F** implants in mice incubated with anginex conjugated nanobins with and without pre-exposure to radiation (3 Gy). ***, $P < 0.001$.

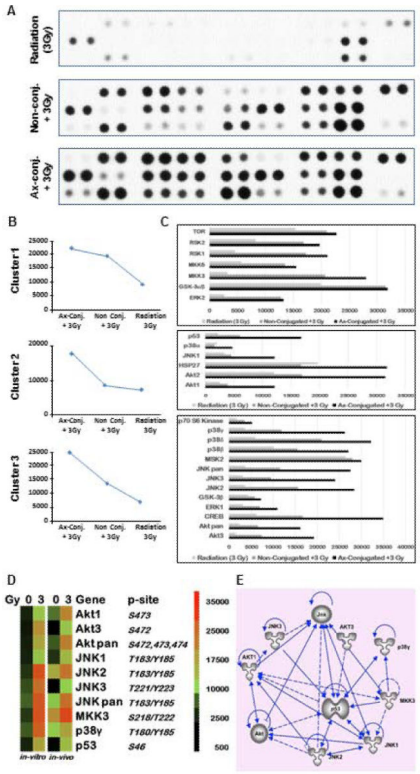

Figure 7. Elevated expression of phospho proteins in the apoptotic and stress signaling pathway in response to targeted nanobins following radiation exposure (3Gy) in TTA and their orthotopic implants in nude mice

(A) A Phospho-MAPK antibody array was used to detect the changes in phosphorylated proteins in TTA (T+E+F) upon radiation exposure and incubation with Ax-conjugated or non-conjugated nanobins after radiation exposure (3Gy). **(B)** Based on the pixel densities of the signal in each spot of the array corresponding to the respective phosphorylated protein, they were grouped in one of the three clusters. **(C)** Quantification of pixel density as a measure of protein phosphorylation in the three clusters. **(D)** Heatmaps comparing the expression of the phosphorylated proteins in the TTA ***(in vitro)*** and upon treatment with anginex-conjugated nanobins with and without radiation exposure. Similar response is observed in tumor tissues at 24 hr post-treatment derived from orthotopic implants of TTAin nude mice ***(in vivo)*****. (E)** Ingenuity pathway analysis showing interaction and regulation of phospho proteins significantly activated in response to the nanotherapeutic treatment strategy by the phosphorylation of functional p53 (S46) that is expected to be activated by the galectin-1 targeting of endothelial cells.